First Results of Gas-Puff Imaging of Edge Turbulence in the W7-X Stellarator

S.B. Ballinger[1], S.G. Baek[1], C. Killer[2], A. von Stechow[2], J.L. Terry[1], O. Grulke[2,3], and the W7-X Team

[1]*Massachusetts Institute of Technology, Cambridge, MA, USA;* [2]*Max Planck Institut für Plasmaphysik, Greifswald, Germany;* [3]*Technical University of Denmark, Lyngby, Denmark*

Background The dynamics of filaments in the scrape-off layer (SOL) of the W7-X stellarator are important to understand turbulence and transport in this region. Several diagnostics on W7-X have characterized filaments and drift effects in the SOL, finding mainly poloidal propagation consistent with the $\mathbf{E}_r \times \mathbf{B}$ drift, with velocities of several km/s [1, 2, 3, 4, 5, 6]. These are complemented by a new gas-puff imaging (GPI) diagnostic, which offers 2D, high time-resolution, toroidally localized recordings of turbulent structures. Two supersonic nozzles puff neutral hydrogen or helium gas locally at the outboard side of the plasma, and line radiation resulting from the interaction of the boundary plasma with the puffed gas is recorded by an 8×16 pixel avalanche photodiode camera at 2 MHz [7]. We present the first results from the W7-X run campaign OP2.1.

Analysis methods Feature motion is more clearly revealed in GPI recordings by subtracting the running average from each pixel. Features are typically between 1–3 cm in size (figure 1).

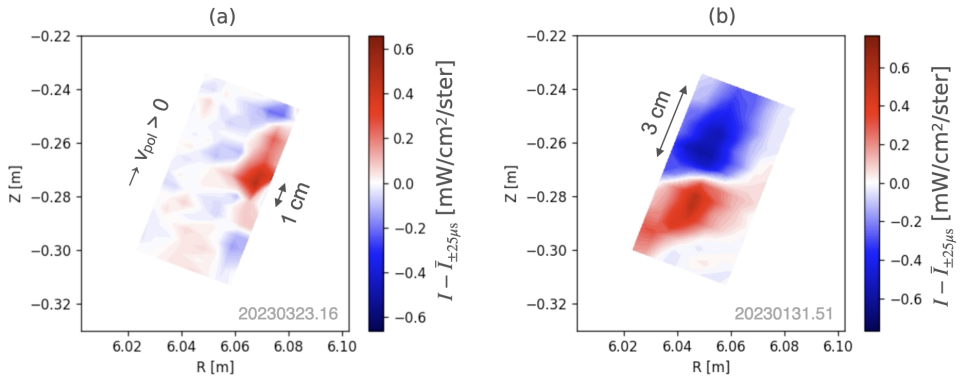

Figure 1: (a) small structures (likely filaments) and (b) large structure (likely a mode) in background-subtracted GPI videos.

Poloidal motion is much more apparent by eye than radial motion in the majority of GPI recordings. Spatio-temporal Fourier analysis is used to estimate the poloidal propagation velocities of features. A frequency-wavenumber spectrum is calculated for each column of pixels, which are oriented so that they are approximately parallel to the last closed flux surface, and coherent phase velocities appear as lines with $\omega = v_{\mathrm{ph}} k$. This spectrum is integrated over ranges

of v_{ph} to create a probability density function (PDF) of phase velocity, and the dominant phase velocity is taken to be that for which the PDF is maximum.

Impact of magnetic field configuration W7-X has a large number of available magnetic configurations, of which the most commonly used are the standard, high mirror, and low and high iota configurations. These were compared by computing the poloidal phase velocity of features moving along each column of the detector over a 50 millisecond period around the time of peak brightness, for all discharges with usable GPI data in forward magnetic field and with any control coil currents. In all configurations, the poloidal speeds evaluated in this way are typically between 1–5 km/s (figure 2(a)). The typical emission fluctuation amplitude is less than 20% of the mean (figure 2(b)). This analysis cannot be used to make blanket statements about the relative amount of edge turbulence in each configuration, as GPI views a different part of the SOL in each one: an island O-point in the standard and high-mirror configurations, an X-point in low iota (figure 3), and the far SOL in high iota. As shown later, the toroidal current also influences the extent of the SOL viewed by GPI, and figure 2 includes measurements at low and high toroidal currents.

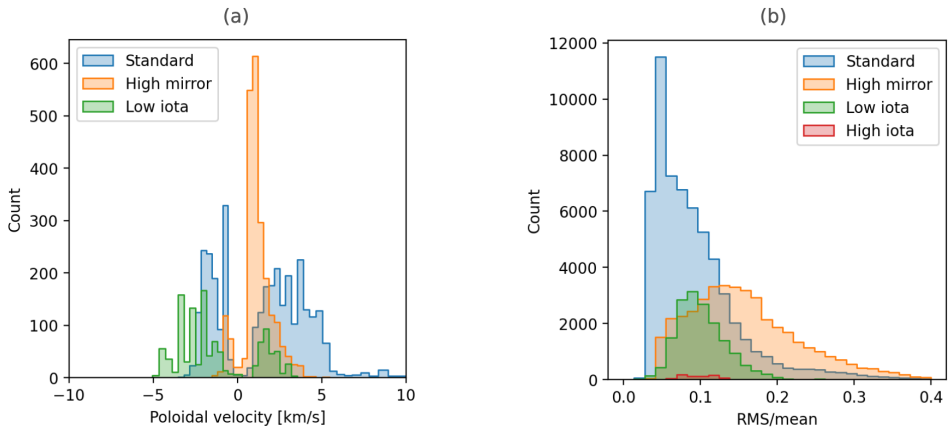

Figure 2: Histograms of (a) the poloidal phase velocity, with the analysis from each column of the detector counted separately and (b) the root mean square divided by the mean, with the analysis of each detector pixel counted separately.

Typical flow patterns As noted earlier, poloidal motion typically dominates radial motion in the fluctuation dynamics. In the standard configuration, with GPI viewing across the O-point of an island, up to 3 shear layers are typically observed in the radial profile of the poloidal velocities (figure 3(a)). When the toroidal field direction is reversed, all these velocities also reverse, offering strong evidence that they are due to the $\mathbf{E}_r \times \mathbf{B}$ drift. The electric potential profile implied by figure 3(a), assuming all velocities are due to $\mathbf{E}_r \times \mathbf{B}$ motion, is qualitatively supported by reciprocating probe measurements of the floating potential under the same conditions.

A series of experiments was performed in which the O-point was moved up and down

poloidally by about ± 11 cm by varying the currents in the control coils: a similar flow pattern is observed when the O-point is moved down below the GPI field of view, but, unexpectedly, approximately all $v_{\mathrm{pol}} > 0$ when the O-point is moved up.

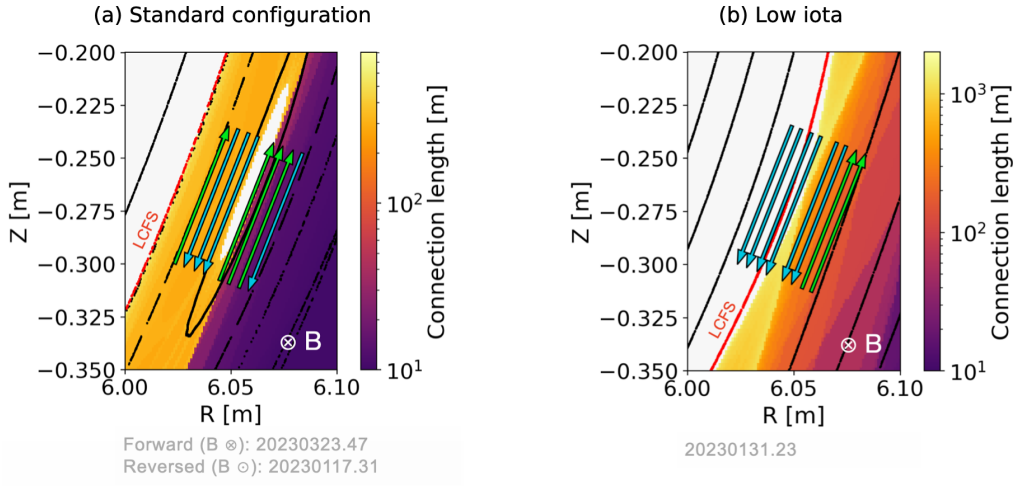

Figure 3: Typical poloidal flow directions of features, determined by Fourier analysis, with arrows spanning each column of the GPI camera detector.

In the low iota configuration, with GPI viewing an X-point and the LCFS, downward poloidal velocities are usually observed on most columns, and upward poloidal velocities on the outermost two columns (figure 3(b)). Occasional radial motion can also be seen in GPI recordings in this configuration.

Impact of toroidal current The toroidal current in W7-X changes the radial position of the magnetic islands [8]. In order to analyze this effect with GPI, all available discharges in the standard configuration with forward field and without control coil currents were used. GPI clearly observes the impact of toroidal current on the radial location of the shear layer, and by implication on the island's radial position: the shear layer from negative to positive poloidal velocity moves toward the plasma center as the toroidal current increases (figure 4(a)). The magnitude of this shift matches those reported in [8]. GPI also observes faster poloidal phase velocities at high toroidal current (figure 4(b)), a phenomenon first observed in W7-X by poloidal correlation reflectometry [1]. Heating power, density, and radiated fraction were not as significantly correlated with poloidal velocities as the toroidal current was, and data from the full ranges of these parameters are shown in figure 4(b). While GPI views more and more of the far SOL as the toroidal current increases, the magnitudes of all detected velocities are affected—GPI does not find feature velocities to be higher or lower in the far SOL compared to the near SOL.

Impact of island size Island size can be varied in W7-X using the control coils. The effect of island size on the poloidal speed of features was analyzed using a series of discharges in the standard magnetic configuration with reversed toroidal field. Figure 4(c) indicates that radially

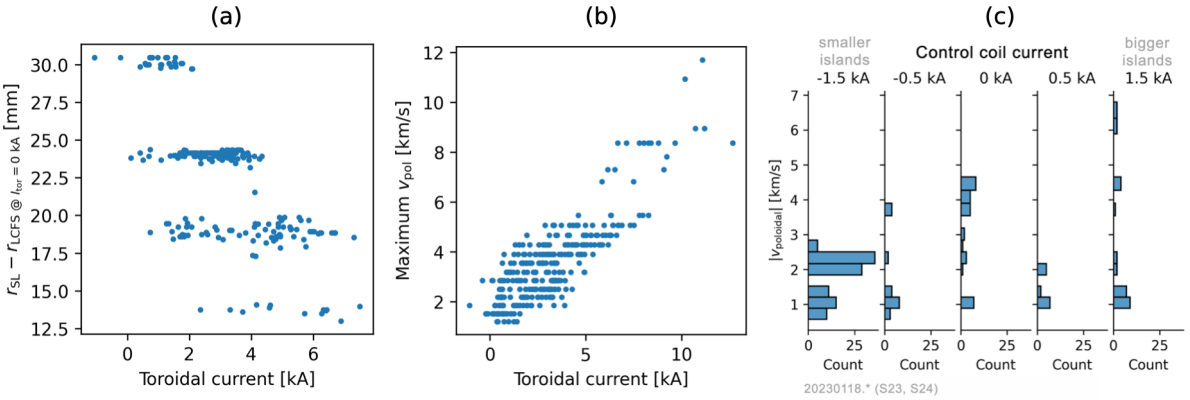

Figure 4: Effects of toroidal and control coil currents in the standard magnetic configuration. (a) Radial distance of the negative-to-positive poloidal velocity shear layer from the LCFS position at $I_{\mathrm{tor}} = 0$ kA as a function of the toroidal current. (b) Maximum poloidal velocity in any column for each GPI recording as a function of the toroidal current. (c) Histograms of the absolute value of the poloidal velocity, counting each detector column separately, for different control coil currents. Positive values of control coil current increase the island radial width, while negative values decrease it.

larger islands have features with higher maximum speeds, implying greater magnitudes of the radial electric field. Another complicating factor is that, as with toroidal current, the change in island size also changes the extent of the island viewed by GPI.

Summary A gas-puff-imaging diagnostic was operated for the first time during the W7-X OP 2.1 campaign, which can measure turbulent transport characteristics across the magnetic islands in the SOL. Features, likely filaments, with diameters ranging from 1–3 cm are seen moving poloidally with typical speeds of 1–5 km/s. Sheared flows are observed across an island O-point with new clarity. Toroidal field reversal experiments offer strong evidence that filament dynamics are dominated by $\mathbf{E}_r \times \mathbf{B}$ motion. Island size and toroidal current are found to affect the velocity profiles observed by GPI.

This work has been carried out within the framework of the EUROfusion Consortium, funded by the European Union via the Euratom Research and Training Programme (Grant Agreement No 101052200 — EUROfusion). Views and opinions expressed are however those of the author(s) only and do not necessarily reflect those of the European Union or the European Commission. Support for the MIT participation was provided by the US Department of Energy, Fusion Energy Sciences, Award DE-SC0014251.

References

[1] A. Krämer-Flecken et al., Plasma Phys. Control. Fusion **61** 054003 (2019)
[2] C. Killer et al., Plasma Phys. Control. Fusion **62** 085003 (2020)
[3] C. Killer et al., Nucl. Fusion **59** 086013 (2019)
[4] D.M. Kriete et al., Nucl. Fusion **63** 026022 (2023)
[5] E. Maragkoudakis et al., Nucl. Fusion **63** 026011 (2023)
[6] S. Zoletnik et al., Plasma Phys. Control. Fusion **62** 014017 (2020)
[7] J.L. Terry et al., Bulletin of the American Physical Society, NP11.00043 (2022)
[8] C. Killer et al., Plasma Phys. Control. Fusion **61** 125014 (2019)